THESIS FOR THE DEGREE OF LICENTIATE OF ENGINEERING

Synthetically simple conjugated polymers for organic electrochemical transistors

Joost Kimpel

CHALMERS

Department of Chemistry and Chemical Engineering

Division of Applied Chemistry

CHALMERS UNIVERSITY OF TECHNOLOGY

Göteborg, Sweden, 2024

Synthetically simple conjugated polymers for organic electrochemical transistors

Joost Kimpel

Thesis for the degree of Licentiate of Engineering

Nr. 2024:06

Department of Chemistry and Chemical Engineering
Division of Applied Chemistry
Chalmers University of Technology
SE-41296 Göteborg

Phone: +46 (0)31 772 1000

Cover:

Leftover conjugated polymer solutions on the spinner after spin-coating polymer films

Chalmers Reproservice

Göteborg, Sweden, 2024

This project has received funding from the European Union's Horizon 2020 research and innovation programme under the Marie Skłodowska-Curie grant agreement No 955837

Synthetically simple conjugated polymers for organic electrochemical transistors

ABSTRACT

The soft and flexible nature of organic materials makes them suitable for the integration into wearable or implantable devices. This paves the way for the development of next-generation bioelectronic systems for e.g. medical diagnostics. Most devices in circuitry can be successfully mimicked by using one or multiple organic electrochemical transistors (OECTs). OECTs leverage the ionic nature of electrolytes in most biological systems, which makes them ideal candidates for bioelectronics.

A series of novel glycolated thieno[3,2-b]thiophene-based semiconducting copolymers is chosen as active materials in OECTs. This series was synthesized *via* direct arylation polymerization. The synthetic complexity indices (SCIs) of the synthesized compounds are comparable with commercial champion OECT materials, and accordingly the new compounds are deemed suitable for upscaling. The SCI evaluation takes synthetic steps, yield, purification, and hazards into consideration to determine the associated risks and costs for upscaling. Subsequently, the effect of chemical structure, polymer properties, and nanostructure are correlated to the ultimate performance of the materials in OECTs. Evaluation of the OECT figure-of-merit against literature and commercial compounds reveals state-of-the-art performance of the synthesized materials.

The best performing material of the series is further investigated using a newly designed characterization technique for OECTs – small signal analysis. By conventional method, different measurements have to be employed to obtain all parameters. With small signal analysis, multiple different properties of OECTs can be determined with a single measurement. Moreover, small signal analysis showcases greater accuracy compared to conventional techniques.

Keywords: *conjugated polymers, direct arylation polymerization, synthetic complexity index, organic electrochemical transistors*

NOMENCLATURE

BBDD	bisthiophenylbenzodithiophenedione
BDD	benzodithiophenedione
BT	benzothiadiazole
C	capacitance
C^*	volumetric capacitance
CV	cyclic voltammetry
Đ	dispersity
E_{ox}	oxidation potential
d	active-layer thickness
DAP	direct arylation polymerization
DFT	density functional theory
DPP	diketopyrrolopyrrole
EIS	electrochemical impedance spectroscopy
F	fluorene
G	conductivity
g_3TT	3,6-bis(triethylene glycol monomethyl ether)thieno[3,2-*b*]thiophene
GIWAXS	grazing incidence wide-angle X-ray scattering
g_m	transconductance
g_m^*	dimension-normalized transconductance
HOMO	highest occupied molecular orbital
I_{on}	on-current
I_{on}/I_{off}	on/off-current ratio
I_{DS}	drain-source current
I_{GS}	gate-source current
IDT	indacenodithiophene
KO*t*Bu	potassium *tert*-butoxide
L	channel length
ITO	indium tin oxide
NC	number of columns

NDI	naphthalenediimide
NH	number of hazard codes
NMR	nuclear magnetic resonance
NO	number of operations
NSS	number of synthetic steps
M_n	number-average molecular weight
MW	molecular weight
OECT	organic electrochemical transistor
OMIEC	organic mixed ionic-electronics conductor
P3HT	poly(3-hexylthiophene)
PBTTT	poly[2,5-bis(3-tetradecylthiophen-2-yl)thieno[3,2-b]thiophene]
PEDOT	poly(3,4-ethylenedioxythiophene)
PEDOT:PSS	poly(3,4-ethylenedioxythiophene):poly(styrene sulfonate)
q	charge
RY	reciprocal yield
SEC	size-exclusion chromatography
SCI	synthetic complexity index
T	thiophene
T2	bithiophene
TT	thieno[3,2-b]thiophene
UV-vis	ultraviolet-visible
V_{DS}	drain-source voltage
V_{GS}	gate-source voltage
V_T	threshold voltage
w	channel width
μ	mobility
σ	conductivity
τ_e	transit time

PUBLICATIONS

This thesis consists of an extended summary of the following appended papers:

Paper I **Synthetically Nimble High-Mobility Organic Mixed Conductors via Direct Arylation Polymerization**

Joost Kimpel, Youngseok Kim, Jesika Asatryan, Jaime Martín, Renee Kroon, and Christian Müller

Under review, **2024**

Paper II **Small Signal Analysis for Organic Electrochemical Transistor Measurements**

Youngseok Kim, Joost Kimpel, Alexander Giovanitti, and Christian Müller

Manuscript in preparation, **2024**

The author has published the following papers which are not included in the thesis:

Paper III **A Route to Conjugated Monomers and Polymers Incorporating 2,5-Connected Oxazole in the Backbone**

Joost Kimpel, Waner He, Ye Cheng, and Tsuyoshi Michinobu

Journal of Organic Chemistry, **2022**, 87, 14, 9384–9390

Paper IV **Block Poly(carbonate-ester) Ionomers as High-Performance and Recyclable Thermoplastic Elastomers**

Georgina L. Gregory, Gregory S. Sulley, Joost Kimpel, Matylda Łagodzińska, Lisa Häfele, Leticia Peña Carrodeguas, and Charlotte K. Williams

Angewandte Chemie International Edition, **2022**, 61, e202210748

Paper V **On the Conformation of Dimeric Acceptors and Their Polymer Solar Cells with Efficiency over 18 %**

Jingnan Wu, Zhaoheng Ling, Leandro R. Franco, Sang Young Jeong, Zewdneh Genene, Josué Mena, Si Chen, Cailing Chen, Prof. C. Moyses Araujo, Prof. Cleber F. N. Marchiori, Joost Kimpel, Xiaoming Chang, Furkan H. Isikgor, Qiaonan Chen, Hendrik Faber, Yu Han, Frédéric Laquai, Maojie Zhang, Han Young Woo, Donghong Yu, Thomas D. Anthopoulos, and Ergang Wang

Angewandte Chemie International Edition, **2023**, 62, e202302888

Paper VI **Impact of Oligoether Side-Chain Length on the Thermoelectric Properties of a Polar Polythiophene**

Mariavittoria Craighero, Jiali Guo, Sepideh Zokaei, Sophie Griggs, Junfu Tian, Jesika Asatryan, Joost Kimpel, Renee Kroon, Kai Xu, Juan Sebastian Reparaz, Jaime Martín, Iain McCulloch, Mariano Campoy-Quiles, and Christian Müller

ACS Applied Electronic Materials, **2023**

Paper VII **Impact of Doping on the Mechanical Properties of Conjugated Polymers**

Sri Harish Kumar Paleti, Youngseok Kim, Joost Kimpel, Mariavittoria Craighero, Shuichi Haraguchi, and Christian Müller

Chemistry Society Reviews, **2024**, Advance Article

CONTRIBUTION REPORT

Paper I	Main author. Conceived the study and wrote the manuscript. Carried out the synthesis, single crystal X-ray diffraction, polymer characterization, UV-vis spectroscopy, cyclic voltammetry, and DFT calculations, as well as associated data analysis.
Paper II	Co-author. Synthesized materials necessary for the study. Aided in conceptualization of measurements in chemical context.

TABLE OF CONTENT

Chapter 1 Introduction

1.1 Organic electronics and bioelectronic systems

Currently standing at a market value of $82 billion with a forecast of $444 billion in 2030, the organic electronics market shows no signs of slowing down its growth.[1] Owing to their flexibility, lightweight, and low-cost of manufacturing, organic electronics are an attractive component for devices such as photovoltaics, light emitting diodes, and thermoelectric generators.[2-4] A more recent application of organic electronics is in the field of bioelectronics.

Compared to inorganic systems, biological tissue is generally more compatible with organic electronics in various bioelectronic applications.[5] The soft and flexible nature of organics makes them suitable for the integration into wearable or implantable devices paving the way for the development of next-generation bioelectronic systems (see Figure 1).[6] The versatility and adaptability of organic electronics position them as key components in the advancement of e.g. medical diagnostics, aiming to evaluate the complexity of biological systems.

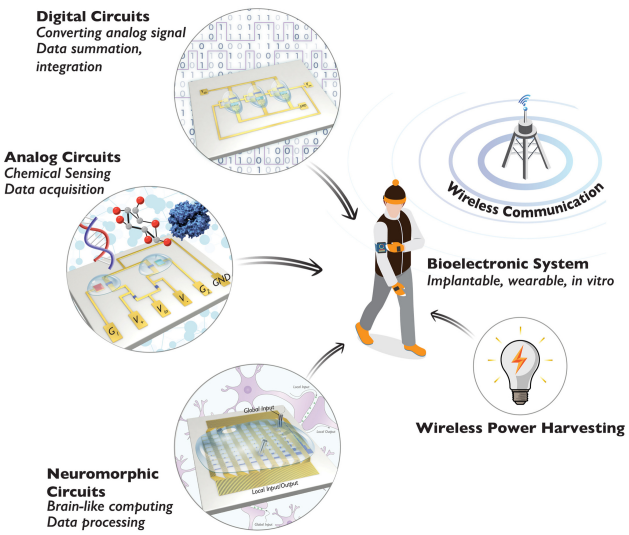

Figure 1. Potential integration of organic electronics in biological applications. Reproduced with permission from reference [6] published by Elsevier.

The organic neuromorphic device is a recent case that showcases the viability of bioinspired devices using soft organic electronics. Neurons operate by the generation of an action potential across the cell membrane, which is accommodated by the transport of ions across the membrane. By creating a circuit based on inverters and S-shaped negative differential resistances with electrically-active organic polymer PEDOT:PSS as the active channel material, a working and implantable mimic of a neuron has been created and used for ion-sensing.[7]

Most devices in circuitry (e.g., the aforementioned inverters) can be successfully mimicked by using one or multiple organic electrochemical transistors (OECTs). Just like ordinary transistors, OECTs switch and/or amplify signals. However, unlike their silicon-based counterparts, OECTs rely on the modulation of ionic currents within the organic semiconductor using the (de-)doped state induced by a potential. This makes them viable candidates for bioelectronics as they can leverage the ionic nature of electrolytes in most biological systems.

1.2 Aim and scope

This thesis presents the synthesis of novel thieno[3,2-b]thiophene-based copolymers through direct arylation polymerization (DAP). Subsequently, their properties as organic mixed ionic–electronic conductors (OMIECs) in organic electrochemical transistors (OECTs) are evaluated.

A glycolated thieno[3,2-b]thiophene monomer is copolymerized with a selection of different comonomers to scope the potential of direct arylation polymerization for this unit (**paper I**). The effect of chemical structure, polymer properties, and nanostructure are correlated to the ultimate performance of the materials in OECTs. These materials are also compared against literature compounds and commercial compounds, and subsequently assessed for their upscaling potential with the synthetic complexity index (SCI).

The OECT performance of the one of the materials, poly(3,6-bis(triethylene glycol monomethyl ether)thieno[3,2-b]thiophene-*co*-bithiophene), is then evaluated in a novel analysis technique for OECTs – small signal analysis (**paper II**). By using this method, multiple different properties can be determined with a single measurement and with greater accuracy compared to conventional techniques.

Chapter 2 Theory

The basics of the function and analysis of organic mixed ionic–electronic conductors and organic electrochemical transistors is discussed, and the relevance of organic semiconductors as the active material highlighted. This is followed by synthetic protocols to organic semiconductors and considerations of complexity of synthesis.

2.1 Organic mixed ionic-electronic conductors and organic electrochemical transistors

Owing to their ability to exploit specific ionic–electronic coupling of organic semiconductors in aqueous electrolytes, the organic mixed ionic–electronic conductor (OMIEC) is an important class of active materials in bioelectronics, energy harvesting and energy storage.[8-11] The OMIEC allows for ions to be coupled with charge carriers inside the material by the electrochemically induced potential through the electrolyte. Accordingly, charge carrier density and corresponding charge carrier mobility can be modulated upon the electrochemical bias. Organic electrochemical transistors (OECTs) use OMIECs as channel materials, thus providing a device architecture to determine the OMIEC properties of materials.[12-15]

The OECT consists of an OMIEC active channel which connects a source and a drain electrode, in the presence of a gate electrode. The active channel is submerged in an electrolyte solution of e.g. NaCl or KCl. The solution is held in place by a polydimethylsiloxane- or glass reservoir. The gate electrode is put into the system either by suspending it into the solution (as in Figure 2) or by coating the substrate with an additional isolated electrode serving as the gate. The electrolyte acts as an interface between the gate and the active material, using the electrolyte to reach high ionic mobilities while concomitantly doping (introduction of charge carriers, accumulation-mode OECT) or de-doping (removal of charge carriers, depletion-mode OECT) the active material.[16]

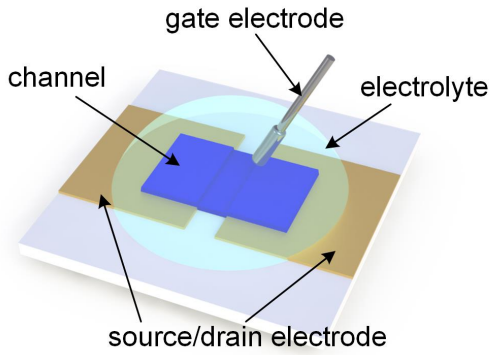

Figure 2. Conventional architecture of OECTs Adapted from paper VII.[17]

2.2 Device characterization techniques of organic electrochemical transistors

Fast switching with high on/off current ratio and a large amplification of input signals are essential in creating a viable OECT device. To probe these characteristics, the product of the charge carrier mobility μ (the velocity of charged carriers upon electric field) and electrochemical volumetric capacitance C^* (the efficiency to accumulate charged carriers on the film) is used as the figure-of-merit. Together with the on-current I_{on}, on-off current ratio I_{on}/I_{off}, and transconductance g_m (a quantification of the amplification of a signal), these parameters describe the basic operation of transistor devices.[18]

OECT devices showcase different characteristics based on the operating regime and accordingly different information is extracted from different situations. The OECT can be in a linear regime (linear dependence drain-source current I_{DS} and drain-source voltage V_{DS}) or in the saturation regime (saturation of I_{DS} with respect to V_{DS}). The condition the device resides in during the measurement dictates the assessment. One set of evaluations is performed for the OECT's steady-state characteristics (saturated response at constant input potential). Another set of evaluations is performed to probe the transient characteristics (response from time-varied input potentials) of the OECT, seeing that it takes time for ions to penetrate the material. For the latter, electrochemical impedance spectroscopy (EIS) is simultaneously performed since it is a prerequisite of the transient response analysis. Both techniques are briefly described in Table 1. The accuracy of these measurements is dubious, due to an inherent dependence of the mobility on the voltage, parasitic resistances included in the response and limited charge transport at low doping levels.[19, 20]

Table 1. Characterization regimes and methods of OECT devices. [a]Parameters extracted either directly from the measurement or by subsequent calculations.

	What is done in the measurement?	Quantified parameters[a]
Steady-state	**Output curves**: I_{DS} probed as a function of changing V_{DS} under various constant gate-source voltages V_{GS}. **Transfer curves**: I_{DS} probed as a function of changing V_{GS} under constant V_{DS} in the saturation regime determined by the output curve.	Threshold voltage (V_T) ON/OFF ratio Transconductance (g_m) Figure of merit (μC^*)
Transient	**Drain-current response**: A V_{GS} pulse with a constant bias is applied until I_{DS} saturates. This is done at a constant V_{DS} in the saturation regime. The V_{GS} pulse is stopped and I_{DS} relaxed to its zero-value. **Transconductance response**: A sinusoidal V_{GS} pulse is applied at a constant V_{DS} in the saturation regime. The frequency of the V_{GS} pulse is changed from 0.1 to 10,000 Hz (part of EIS measurement).	Transit time (τ_e) ON/OFF ratio Transconductance (g_m) Figure of merit (μC^*) Capacitance (C) from EIS

In **paper II**, a novel technique for analyzing OECTs is explored. There is an inherent problem to correlate the results between the steady-state and transient characterization since the device is operated in different situations. Nonetheless, the results are still correlated. To avoid doing multiple measurements and to properly correlate results, small signal analysis can be employed to simultaneously get the steady-state and transient response.[21] By imposing a small alternating current signal (frequency range around 10 Hz) during the voltage sweep, the steady-state and the transient response are acquired simultaneously. The voltage sweep can be thought of as the steady-state response, whereas the small signal is the transient response (Figure 3a). This theory expands further since the small signal application allows for the separation of real and imaginary parts of output currents (which stand for the redox and capacitive response, respectfully) by a Phasor plot (Figure 3b). This allows for the separation of parasitic components in the response. Ultimately, this yields a measurement where all device properties can be determined from a single measurement, which has not been possible before (Section 4.5).

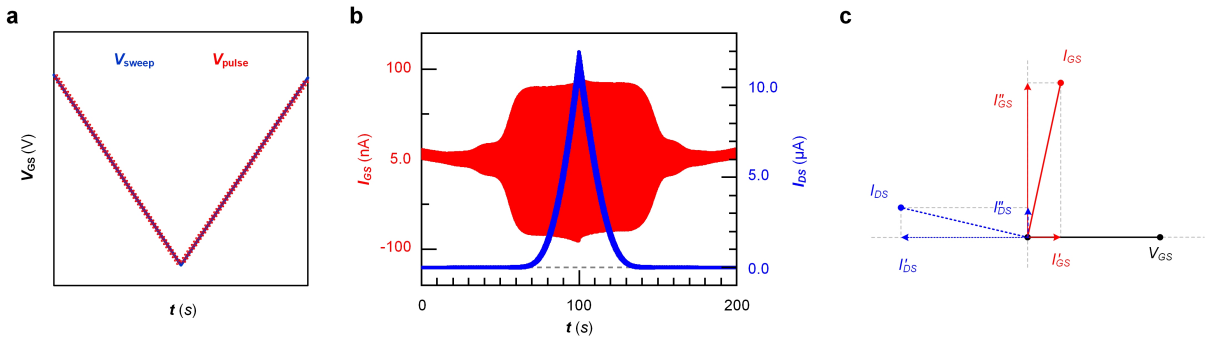

Figure 3. Simplified model of small signal analysis in (a) showcasing the assigned input voltage signal, with the measured output currents in (b) and corresponding Phasor diagram in (c). Adapted from paper II.

2.3 Design of conjugated polymers for OECTs

Aromatic π-conjugated polymers are a class of organic semiconductors often applied as the active OMIEC materials in OECTs.[22-24] They are an attractive class owing to their high tunability through synthesis or the use of additives. Different polarities of devices (i.e. hole-transporting/p-type or electron-transporting/n-type) can be made by using different conjugated polymers. On top of that, by specific design, conjugated polymers can mimic softer tissue present in the body which makes potential of implantation more viable.

Polyacetylene is the simplest conjugated polymer, featuring alternating single and double bonds throughout. By substituting aromatic units into the backbone, this conjugated pattern is maintained whilst simultaneously altering the energy landscape of the orbitals. This changes the character of the polymer from p-type to n-type. Some common aromatic units, which can be electron-donating (p-type) or electron-withdrawing (n-type), incorporated in conjugated polymers are thiophene, fluorene, and naphthalenediimide.

The π-system is conjugated through the entire polymer. Therefore, these polymers are rigid and tend to aggregate due to π-π stacking. This improves charge hopping between different chains and within the percolated path but makes processability of the materials complex. To improve the processability, units are donned with solubilizing side chains. Side chains are linear single chains or (multi-)branched and can be aliphatic, oligoether, or ionic in nature.[25-27] Which side chain is required depends on the processing solvent and ultimate application. However, a balance must be found between processability and performance – side chains with too much conformational entropy negatively impact the ordering in the microstructure, and so the charge carrier mobility, of the polymer.[28-30]

In OECTs, the polymer must be able to respond to the bias created through the electrolyte. Since the backbone of the polymer consists of (mostly) apolar units, the side chains must accommodate for the response and subsequent insertion and movement of ions. Accordingly, oligoether side chains are a good candidate for both p- and n-type devices, since the polarity imparted by the oligoether chain aids the stabilization of the ions. The Coulombic interactions of the side chain also help shield the charge created on the polymer and the ion thus improving transport properties. In this work, p-type devices are targeted. This makes oligoether side chains even more attractive. By attaching the oligoether side chain through the oxygen to the polymer backbone, the highest occupied molecular orbital (HOMO) level is raised and the oxidation potential lowered.[31]

2.4 Synthesis of conjugated polymers

The simplest form of a conjugated polymer would take a conjugated small molecule and polymerize it with itself, creating the homopolymer (see Figure 4a). This can be achieved by electropolymerizing the unit from a substrate/electrode or by chemical oxidative polymerization. In both methods, a radical cation is created, due to the abstraction of an electron, which initiates chain growth. These methods are commonly employed to synthesize unsubstituted conjugated polymers, such as polyaniline and poly(3,4-ethylenedioxythiophene) (PEDOT).[32, 33] A common synthetic route to obtain poly(3-alkylthiophenes), e.g. P3HT, is by homopolymerization of thiophene by Grignard metathesis polymerization, by *in situ* creation of a Grignard reagent.[34]

More complex conjugated polymers can be realized through the combination of two monomers, by using cross-coupling polycondensation methods (see Figure 4b). Aryl halides and pre-functionalized monomers are coupled by using an organometallic catalyst such as in Stille coupling or Suzuki coupling. Functionalization makes precursors atom inefficient (Stille, Suzuki) and even toxic (Stille). As an alternative, if monomers possess active aromatic C-H bonds, direct arylation polymerization (DAP) from the unfunctionalized monomer is possible. However, DAP has several challenges to overcome, such as a limited number of suitable monomers that are reactive enough and the lack of C-H regioselectivity leading to defects in regioregularity. A direct comparison between Stille-made materials reveals that DAP-made materials often have lower molecular weights and a greater prevalence of defects.[35, 36]

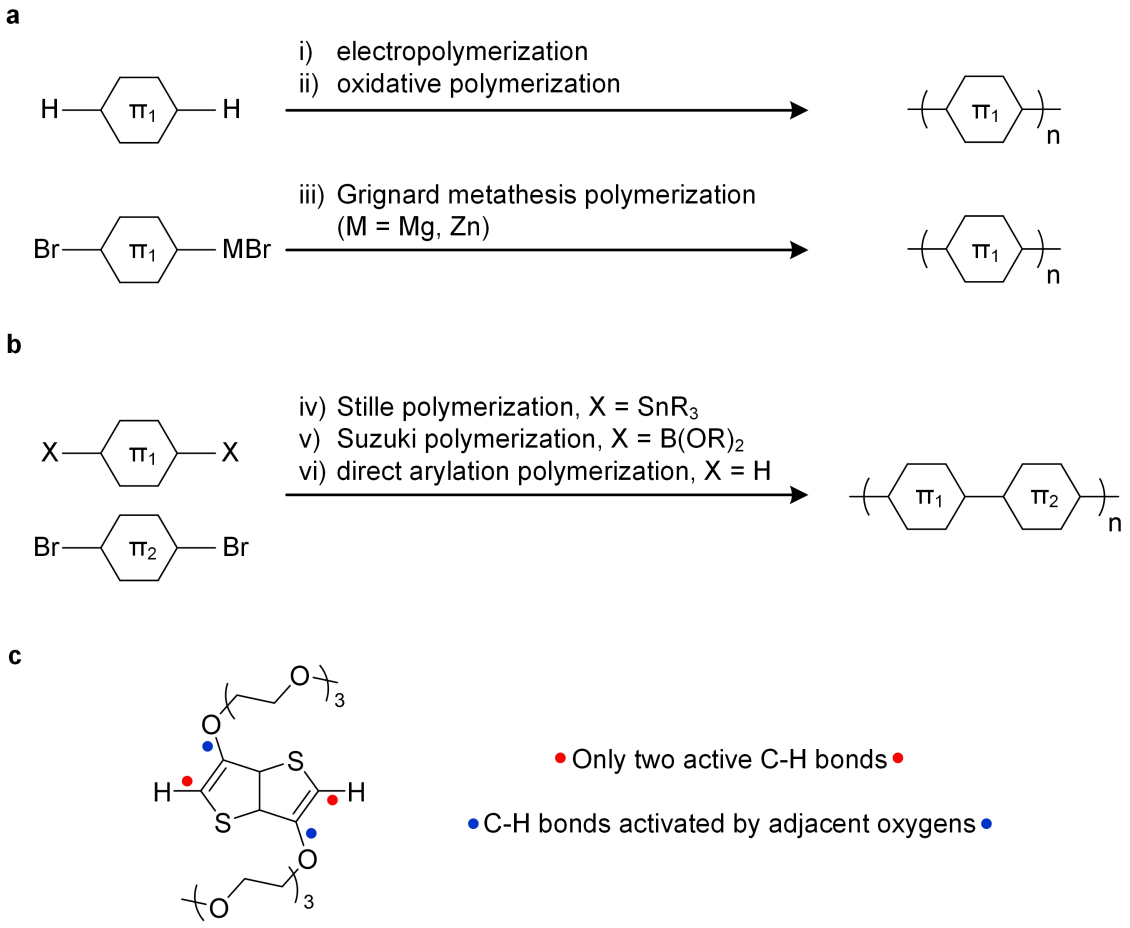

Figure 4. Polymerization methods using (a) a single monomer and (b) two monomers. Monomer design of 3,6-bis(triethylene glycol monomethyl ether)thieno[3,2-*b*]thiophene (g_3TT) in (c). Adapted from paper VII.[17]

The C-H active monomer can be carefully constructed to avoid the formation of defects. By creating a highly active monomer, one where the nucleophilicity stands orthogonal to the electrophilicity of the brominated monomer, homocoupling defects (self-coupling of aromatic units) can be mitigated. β-defects, reaction of unwanted C-H one position away from the desired reaction position, can be fully eliminated by blocking any other reactive C-H by. For instance, a commonly chosen unit for DAP is 1,2,4,5-tetrafluorobenzene, seeing that it only has two C-H bonds.[37] Accordingly, the monomer chosen for this study is 3,6-bis(triethylene glycol monomethyl ether)thieno[3,2-*b*]thiophene (g_3TT) (see Figure 4c), which has only two C-H bonds that can react and these two C-H bonds are highly activated due to the strong donating character of oxygens in the monomer.[38]

2.5 Synthetic complexity index

Conjugated polymers open the road to a myriad of applications, such as bioelectronics, energy harvesting and energy storage, owing to their soft nature and semiconducting characteristics. High-performance devices require high-end materials which tend to suffer from long syntheses, low yields, and many hazardous materials in the process.[8, 39, 40] Accordingly, the route to these materials seems paradoxical due to the (biologically) harmful compounds used and energy input required to make the materials. This is especially true considering the potential of underperformance of novel compounds having gone through an arduous synthesis process (see Figure 5).

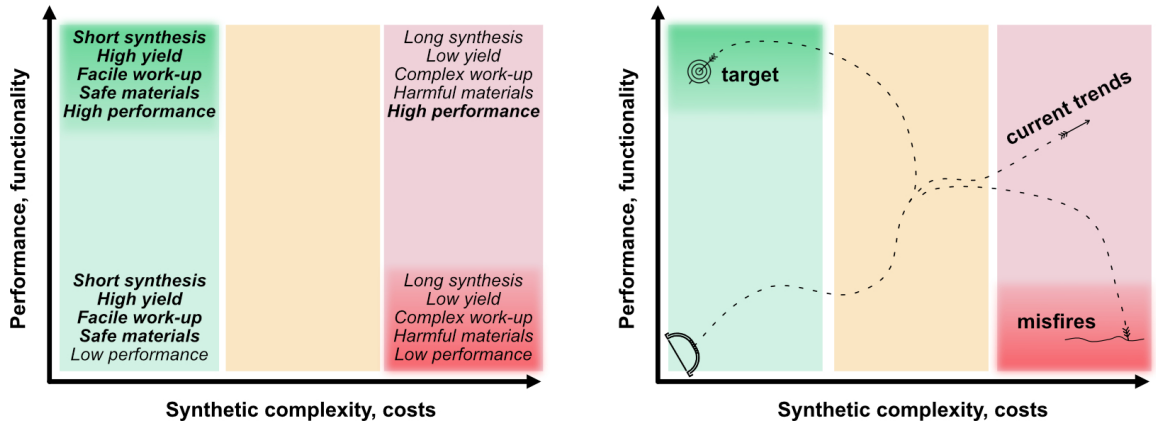

Figure 5. Representation of desired performance and synthetic complexity index. The organic electronics field is plagued with long syntheses processes which use harmful chemicals and laborious purification procedures.

In an attempt to address this, Po *et al*. described a method to evaluate the potential of upscaling of materials through the synthetic complexity index (SCI).[41] The normalized SCI is defined as Equation 1:

$$SCI = \boldsymbol{a} * \frac{NSS}{NSS_{max}} + \boldsymbol{b} * \log\left(\frac{RY}{RY_{max}}\right) + \boldsymbol{c} * \frac{NO}{NO_{max}} + \boldsymbol{d} * \frac{NC}{NC_{max}} + \boldsymbol{e} * \frac{NH}{NH_{max}} \quad (1)$$

where NSS is the number of synthetic steps, RY is the reciprocal yield of the total yield, NO is the number of operations (quenching, precipitation, extraction, filtration/plug, recrystallization, Soxhlet, dialysis, and centrifugation), NC is the number of flash columns or preparative HPLC, and NH is the number of hazard codes with the most severe classification.

All numbers are compared against the maximum (max subscript) of each step in the list of compounds considered. The higher the number of a parameter, the more unfavorable the step. The coefficients **a** – **e** are assigned semi-empirically according to overall cost and safety, leading to Equation 2:

$$SCI = 35 * \frac{NSS}{NSS_{max}} + 25 * \log\left(\frac{RY}{RY_{max}}\right) + 15 * \frac{NO}{NO_{max}} + 15 * \frac{NC}{NC_{max}} + 10 * \frac{NH}{NH_{max}} \quad (2)$$

Chapter 3 Experimental

Specifics of chemicals used, synthetic protocols followed, and characterization techniques employed are succinctly described. More detailed explanations can be found in the appended works.

3.1 Materials

General

Triethylene glycol monomethyl ether, potassium *tert*-butoxide, copper(I) iodide, amine ligands, hydroxide bases, pivalic acid, cesium carbonate, tris(dibenzylideneacetone)dipalladium(0)-chloroform adduct and sodium diethyldithiocarbamate trihydrate were received from Sigma Aldrich and VWR and used without further purification. Analytical grade hexane, ethyl acetate, diethyl ether, methanol, and chloroform were obtained from Fisher Scientific and used as received. Analytical grade toluene and tetrahydrofuran were purchased from Fisher Scientific, dried, charged into a solvent purification system, and directly taken as required. The precursor to the monomer, 3,6-dibromothieno[3,2-b]thiophene (BLDpharm, 98%), was obtained through Chemtronica.

Dibrominated comonomers

Dibrominated comonomers were all commercially available and obtained from various vendors such as VWR, Sigma, and JiangSu GR-Chem Pharma Technology Ltd. If purity was below 98%, solid comonomers were recrystallized from pentane or methanol in the freezer at -20 °C and dried before use. 2,5-Dibromothiophene was purified through distillation before use.

3.2 Synthetic details

Monomer synthesis and work-up

3,6-Bis(triethylene glycol monomethyl ether)thieno[3,2-b]thiophene (g_3TT) was synthesized by Ullmann coupling of triethylene glycol monomethyl ether to 3,6-dibromothieno[3,2-b]thiophene, using copper(I) iodide as catalyst and deprotonated glycol as the nucleophile. After the reaction and subsequent work-up by neutralization, filtration, extraction, and a flash column, a crude brown oil was obtained. This was recrystallized in cold diethyl ether yielding yellow crystals. A detailed synthetic protocol to g_3TT is described in the supporting information of **paper I**.

Polymer synthesis and work-up

The polymers were synthesized through direct arylation polymerization. To a vial under inert atmosphere, the brominated aromatic monomer and the hydrogen source aromatic monomer were mixed in a 1:1 ratio. To this same vial, pivalic acid, cesium carbonate, tris(dibenzylideneacetone)dipalladium(0)-chloroform adduct and toluene were added. This was then heated to 110 °C until completion of the reaction. The reaction was monitored by precipitation of the reaction mixture into various solvents. Upon completion, the reaction mixture was collected, precipitated, filtered, and collected in a Soxhlet thimble to ultimately perform Soxhlet with hexane, methanol, ethyl acetate and chloroform. The highest molecular weight fraction was collected. A more detailed synthetic protocol for the polymerizations can be found in the supporting information of **paper I**.

3.3 Characterization of monomer

Nuclear magnetic resonance (NMR) techniques

The monomer structure was confirmed through 1D (^{1}H and ^{13}C) and 2D (COSY, HSQC, HMBC) nuclear magnetic resonance (NMR) spectra. Spectra were recorded on a Bruker Avance NEO 600 spectrometer. Where relevant, ^{1}H and ^{13}C NMR spectra were referenced to the residual solvent peak ($CDCl_3$: $\delta(^1H)$ = 7.26 ppm, $\delta(^{13}C)$ = 77.16 ppm).

Single crystal X-ray diffraction

Atomic positions in single molecule structures can be determined by Fourier transforming the diffraction pattern of a crystal of the small molecule. Despite long, flexible oligoether side chains, large crystals were grown of g_3TT. By mounting the crystals on a nylon loop on an XtaLAB Rigaku Synergy R HyPix diffractometer using CuKα radiation (λ = 1.54184 Å), full diffraction patterns were obtained within minutes. The short data collection time required suggests high quality crystals. Structures were solved using the Intrinsic Phasing solution method and using Olex2 as a graphical interface.[42, 43]

3.4 Characterization of polymers

Molecular weight and end-group fidelity

Molecular weight determination of polymers is performed to assess the efficacy of the polymerization and to corroborate with any material property results. Size-exclusion chromatography (SEC) is a commonly employed technique, where residence time in a gel column is standardized against reference polymers with specific molecular weight. Chromatograms were recorded using an Agilent 1260 Infinity SEC at a temperature of 70 °C, employing two columns and a precolumn containing Polargel M 300 × 7.5 mm with mixed pores and a pore size of 8 µm. Polymer samples were dissolved in dimethylformamide (DMF) at a concentration of about 1 g L^{-1}. The eluent used was DMF with 0.1 wt% LiBr. Owing to the highly polar nature of the synthesized polymers, a polar column was chosen to perform the analysis. Relative calibration was carried out with poly(methyl methacrylate) standards since these have a more similar persistence length as opposed to the more commonly used polystyrene standards.

Polymers were characterized by high-temperature NMR. High temperature is required to ascertain relaxation and to increase resolution/decrease signal broadening. ^{1}H spectra were recorded on a Bruker Avance NEO 600 spectrometer (^{1}H: 600.13 MHz) at 393K in tetrachloroethane-d_2. The ^{1}H and ^{13}C NMR spectra were referenced to the residual solvent peak ($C_2D_2Cl_4$: $\delta(^1H)$ = 5.98 ppm). To our surprise, end-groups could be observed and used to determine polymer molecular weight. This is further explained in Section 4.2.

Structural order

Structural order of a polymer thin film is a major factor in dictating its ultimate behavior in devices. In this work, structural order is mainly addressed through spectroscopic and scattering techniques.

UV-vis spectroscopy provides insight into transitions between energy levels of π electrons in the conjugated polymer. The absorption spectra give information about the optical bandgap (correlated to energetics of monomers and polymer conjugation length), structural order, and oxidation level. Polymer solutions in chloroform with a concentration of 5 - 10 g L^{-1} were prepared and spin-coated onto pre-cleaned and dried glass microscope slides. UV-vis spectra of thin films were recorded with a PerkinElmer Lambda 1050 spectrophotometer. Spectra were normalized by the film thickness obtained with profilometry.

To assess the (presence of) structured domains in the polymer thin films, grazing incidence wide-angle X-ray scattering (GIWAXS) was employed. Ordered chains in the thin film will diffract incoming X-rays in accordance with Bragg's law which provides a pattern that can be translated to assess lamellar stacking and π-stacking in the thin film. Polymer solutions in chloroform with a concentration of 5 - 10 g L^{-1} were prepared and spin-coated onto cleaned and plasma treated silicon wafers. GIWAXS patterns were recorded at the beamline NCD – SWEET of the Alba synchrotron using an X-ray wavelength of 1 Å and a sample detector distance of 201.17 cm. Crystalline structure was analyzed using the Scherrer equation.

Oxidation potential and electrochemical response

For organic mixed ionic-electronic conductors (OMIEC) materials, insertion of ions and creation of charges in the polymer backbone should be facile. For p-type materials, a shallow HOMO level/low oxidation potential is required. Moreover, for ion insertion to occur efficiently, the polymer must be able to swell in water; i.e. to warrant a response as an OMIEC in a bioelectronic context, the material must respond in an aqueous electrolyte. Hence, both the oxidation potentials must be determined and the electrochemical responses assessed in different media.

Cyclic voltammetry (CV) was used to acquire the polymer oxidation potentials. Polymer films were spin-coated from chloroform solutions (5 - 10 g L^{-1}) onto an ITO-coated glass substrate and patterned to a size of ~0.5 cm^2. The exposed ITO layer was passivated with parafilm or epoxy resin. This is done to separate the active layer and the ITO layer. This was connected to a CH instrument CHI 650D using a three-electrode configuration. For the characterization in an aqueous electrolyte (0.1 M $NaCl/H_2O$), an Ag/AgCl reference electrode was used, while in case of a non-aqueous electrolyte (0.1 M, NBu_4PF_6/acetonitrile) an Ag/Ag^+ reference electrode was used. A scan rate of 50 mV s^{-1} was used and scans were performed in the range of -0.4 V to +0.6 V for the aqueous electrolyte and -0.8 V to +0.8 V for the non-aqueous electrolyte. The reference potential E^0 of the electrode was taken as $E^0 = 4.4$ eV for the aqueous electrolyte and $E^0 = 5.1$ eV for the non-aqueous electrolyte. The latter is calibrated against the peak of the ferrocene/ferrocenium (Fc/Fc^+) redox couple. Accordingly, oxidation potentials were calculated by $E_{ox} = \Phi_{ox} + E^0$.

Electrochemical impedance spectroscopy (EIS) is a technique which is used to determine events at electrolyte interfaces. Spectra were recorded in a frequency range from 0.1 to 10,000 Hz, and the offset potential was varied from -0.4 V to +0.6 V vs. Ag/AgCl, in line with the CV spectra. Using EIS Spectrum Analyser software and an equivalent circuit model $R_e[R_sC_s[R_c[R_aC_a]]]$,where R_e, R_s, C_s, R_c, R_a and C_a are the resistance of the electrolyte, electrochemical resistance/capacitance of the ITO substrate, contact resistance between the substrate and the active layer, and electrochemical resistance/capacitance of the active layer, respectively, the electrochemical capacitance of the active layer was extracted.

Computational analysis

Ab initio calculations of oligomers can provide insights into the reason why a polymer exhibits certain material properties. Geometry optimizations to reach stable conformations were performed to obtain information on the polymer such as energy levels, orbital coefficients, and dihedral angles between conjugated units. The ωB97XD functional with 6-31+G(d,p) level of theory was used. Side chains were truncated simplify the calculation. Optimized structures were validated to be 'true' by the lack of imaginary vibrations in vibrational analysis.

3.5 Characterization of devices

Device preparation

Through lithographic techniques, the source and drain metal electrodes were defined, resulting in channels with a width w = 200 μm and length L = 20 μm. Active layers were spin-coated from chloroform solutions (7 g L^{-1}) by spinning the substrate at 1500 rpm and casting the solutions. Thicknesses ranged from 50 to 120 nm. A reservoir was created on top of the active channel to hold the electrolyte (100 mM NaCl). Device characterization was conducted with two MATLAB-controlled Keithley 2400 source-measure units. The gate potential was applied through the electrolyte by using a three-electrode configuration with an Ag/AgCl reference electrode and a platinum wire counter electrode. By using two potentiostats, Keithley 2400 for conventional method and SP300 for the small signal, small signal analysis was performed.

Chapter 4 Results

The synthesis of novel glycolated thieno[3,2-b]thiophene-based copolymers through direct arylation polymerization (DAP) is investigated and the material properties analyzed. In turn, these properties are correlated with performance of the polymers as active materials in organic electrochemical transistors (OECT). Conventional OECT characterization methods are compared against a novel small signal analysis, which combines previous techniques into a single measurement.

4.1 Synthesis of monomer and polymers

Ullmann couplings provide highly efficient reactions between nucleophiles and aromatic cores using inexpensive copper(I) iodide for mediation of the reaction.[44] 3,6-Bis(triethylene glycol monomethyl ether)thieno[3,2-b]thiophene (g_3TT) was successfully synthesized by Ullmann coupling of triethylene glycol monomethyl ether to 3,6-dibromothieno[3,2-b]thiophene (see Figure 6).

Previous syntheses of g_3TT showcased relatively low yields of around 15%.[38] To improve the reaction yield, a range of different solvents, bases, and catalytic additives were employed in the reaction. To circumvent the use of harmful solvents, keeping synthetic complexity (SCI) in mind, the reaction using triethylene glycol monomethyl ether as the reaction medium was attempted. To ascertain enough nucleophilic chains are created, strong, non-nucleophilic, base potassium *tert*-butoxide (KO*t*Bu) is used. The use of cheaper hydroxides in the synthesis was also explored to probe the necessity of the non-nucleophilic KO*t*Bu. Ullmann couplings also benefit from the inclusion of amines to stabilize the copper(I) species, so alongside the solvent and base change, amine ligands were investigated.[44, 45]

Initial attempts employed KO*t*Bu as the base and no amine ligands. The use of the glycol as reaction medium significantly increased the final yield of g_3TT around 50%, more closely resembling the efficiency of Ullmann coupling for thiophene.[31] Amine ligands phenanthroline and sarcosine led to a large decrease in efficacy of the Ullmann coupling. One explanation is

several radical single electron transfer events between the amine and KO*t*Bu creating (di)anionic amine ligand,[46] which is postulated to bind very strongly to inactive copper(II), deactivating the reaction. Changing the base to cesium hydroxide or sodium hydroxide stunted the reaction yield compared to KO*t*Bu. In case hydroxide was used to deprotonate the glycol, a light blue precipitate started to form after several hours. This is indicative of the formation of deactivated copper(II). Ultimately, the reaction was performed using KO*t*Bu with triethylene glycol monomethyl ether as the solvent.

DAP between g$_3$TT and brominated comonomers was performed. Comonomers include the full spectrum of electronic character ranging from donating units (thiophene (T), bithiophene (T2), and thieno[3,2-b]thiophene (TT)), to neutral units (fluorene (F), diketopyrrolopyrrole (DPP), indacenodithiophene (IDT), and bisthiophenylbenzodithiophenedione(BBDD)), to accepting units (benzothiadiazole (BT), benzodithiophenedione (BDD), and naphthalenediimide (NDI)), the polymers of which are further annotated as **P1** – **P10** as shown in Figure 6. Summarized data is presented in Table 2.

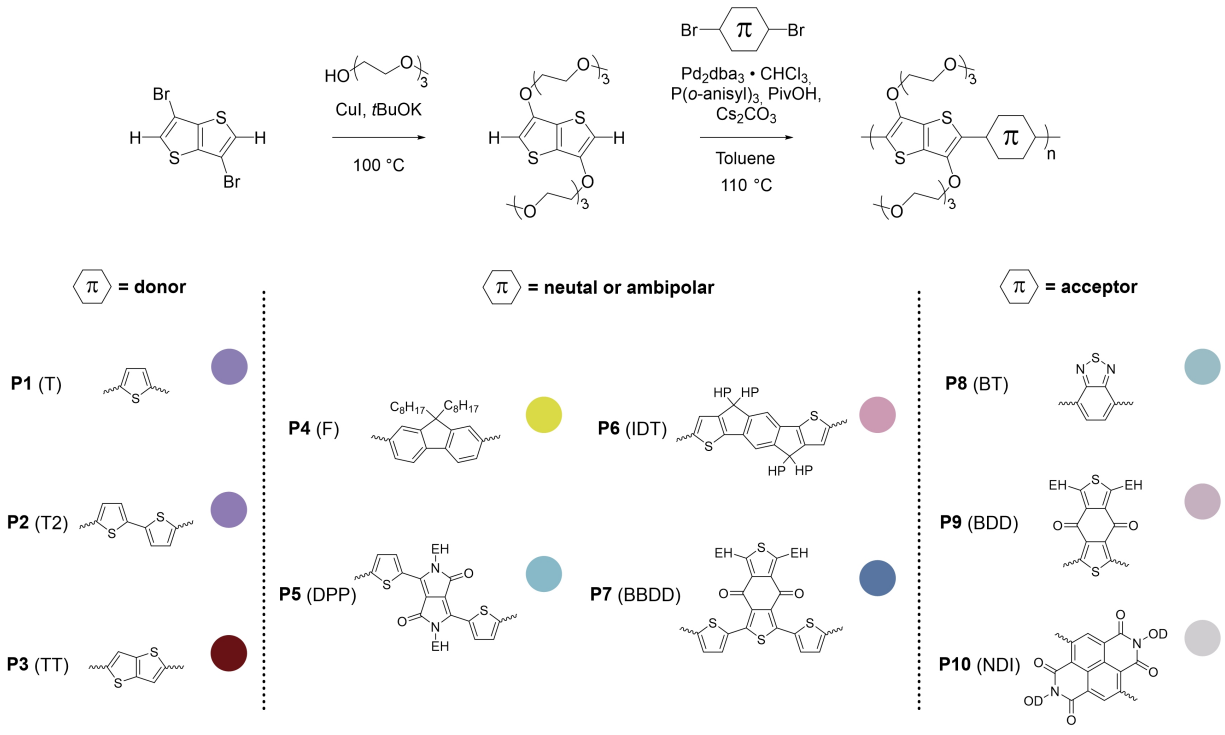

Figure 6. Synthesis of g$_3$TT and direct arylation polymerization (DAP) of g$_3$TT with donor, neutral/ambipolar or acceptor type comonomers. The insets show photographs of thin films of the polymers P1 – P10. EH = 2-ethylhexyl, HP = 4-hexylphenyl, OD = 2-octyldodecyl. Adapted from paper I.

4.2 Polymer characterization and synthetic complexity index determination

The molecular weight was initially determined by size-exclusion chromatography (SEC) in a polar column using dimethylformamide (DMF) with 0.1 wt% LiBr as the eluent. A large range of polymer molecular weights were obtained using DAP under the aforementioned conditions; oligomers for **P5** (DPP) and **P10** (NDI), <10 kg mol^{-1} for **P3** (TT) and **P6** (IDT), and >10 kg mol^{-1} for the others reaching up to 90.5 kg mol^{-1} for **P9** (BDD). No clear trend in molecular weight can be linked to the electronic character of the comonomers. The lower molecular weights can be reasoned by a highly planar one-dimensional chain (**P3**), prevalent defect formation in brominated unit (**P5**), or strong transannular strain of comonomers in the reaction (**P10**). **P8** could not be measured as it did not dissolve in DMF.

In some specific cases throughout literature, end-groups of polymers can confidently be assigned by high-temperature NMR.[47, 48] Hence, the absolute molecular weight can be determined by comparing the end-group signal with the main chain signal. Since g$_3$TT has an indicative aromatic peak at 6.3 ppm which can only exist in case of an end-group, this analysis is possible for the polymers considered in this work. By correlating this signal in a 1:2 ratio to a glycol signal at 4.3 ppm, end-group analysis can be performed by comparing the glycol side chain signals (see Figure 7) and substituting them in Equation 3. The determined values agree with the data extracted by SEC for **P1**-**P4**, **P6** and **P7** (see Table 2).

$$M_{n,NMR} = \frac{MW_{repeat}}{2}\left(\frac{\int I_{chain}\, d\delta}{\int I_{end}\, d\delta} + 1\right) + MW_{HBr} \qquad (3)$$

The synthetic complexity index (SCI) is a stand-alone list which compares the materials in the list for their ease of synthesis, keeping in mind synthetic steps, yield, purification, and hazards.[41] By considering a list of materials created by different synthetic routes, and even commercially available compounds, the synthesis presented can be compared directly and its viability of upscaling evaluated. All materials made in this work have an SCI of circa 30 (see Table 2). This is significantly lower than materials made by Stille coupling (SCI = 36-85),[31, 49, 50] DAP (SCI = 37-59),[38, 51, 52] and even commercially available poly[2,5-bis(3-tetradecylthiophen-2-yl)thieno[3,2-b]thiophene] (PBTTT) (SCI = 37).[53] Materials with lower and similar SCIs are commercial PEDOT,[23] made by oxidative polymerization, and a recently reported material using 3,4-bisoligoether thiophene as a monomer in DAP.[52]

Table 2. Summary of in-depth polymer analysis. P5 and P10 are omitted. [a] Yield from highest molecular weight fraction from Soxhlet extraction, annotated with solvent. [b] Measured by SEC at 70 °C against poly(methyl methacrylate) standards using DMF with 0.1 wt% LiBr as the eluent. [c] Determined by end group analysis from NMR spectra recorded at 120 °C in $C_2D_2Cl_4$. [d] Synthetic complexity determined from a list of 36 materials (commercial and non-commercial). [e] Polymer did not dissolve in DMF with 0.1 wt% LiBr. Adapted from paper I.

polymer	yield (%)[a]	$M_{n,SEC}$ (kg mol^{-1}) [b]	Đ[b]	$M_{n,NMR}$ (kg mol^{-1})[c]	SCI[d]
P1 (T)	65, $CHCl_3$	14	6.4	14	30
P2 (T2)	33, $CHCl_3$	29	2.2	39	33
P3 (TT)	34, $CHCl_3$	5	>10	3	33
P4 (F)	31, EtAc	34	1.7	49	32
P6 (IDT)	27, EtAc	9	1.4	29	33
P7 (BBDD)	50, $CHCl_3$	15	6.3	16	31
P8 (BT)	54, $CHCl_3$	n.a.[e]	n.a.[e]	13	31
P9 (BDD)	67, $CHCl_3$	90	1.3	21	30

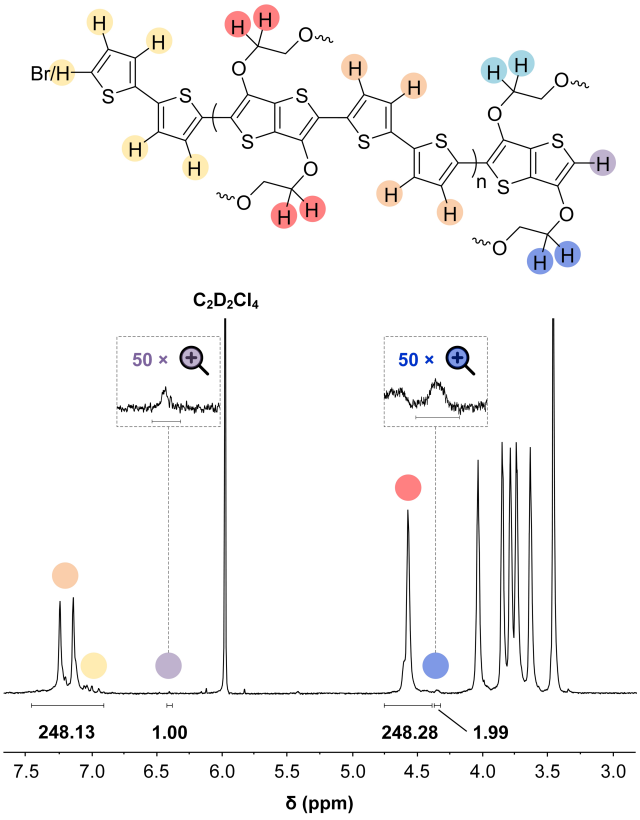

Figure 7. NMR spectrum of p(g_3TT-T2) (P2) recorded in tetrachloroethane-d_2 at 120 °C, allowing end-group analysis by comparing the end-group oligoether CH_2 (blue) and the main chain oligoether CH_2 (red). The signals at circa 6.40 ppm and circa 4.30 are assigned to the aromatic C-H of g_3TT (purple) and the end-group oligoether CH_2 (blue), respectively, because the ratio of the integrated areas is 1:2. Adapted from paper I.

4.3 Electrochemical properties and thin-film nanostructure

Oxidation onset potential E_{ox} of polymer thin films was determined by cyclic voltammetry (CV). Chloroform solutions were deposited onto ITO substrates and an effective area created by cleaning the substrate with a cotton swab soaked with chloroform. Voltammograms were recorded in both non-aqueous (0.1 M NBu_4PF_6 in acetonitrile) and aqueous (0.1 M NaCl in H_2O) electrolyte. Different electrolytes are checked to probe the potential application in organic electrochemical transistors (OECTs), as these operate primarily in aqueous electrolyte with the ultimate application as bioelectronics.[16]

In non-aqueous electrolyte, E_{ox} ranged from circa 4.7 eV to 5.7 eV. Polymers of g_3TT with small comonomers such as **P1** (T), **P2** (T2), **P3** (TT) and **P8** (BT), showcased shallow HOMO levels of around 4.75 eV attributed to the dominant donating character of g_3TT. Exemplar voltammograms are shown in Figure 8a. Larger comonomers in **P4** (F), **P5** (DPP), **P7** (BBDD) and **P9** (BDD) had a bigger effect on E_{ox}. These showcased similar values to the homopolymers of the brominated comonomer or strongly shifting it beyond due to the strong accepting character of the brominated comonomer. In aqueous electrolyte, only **P1**, **P2**, **P3**, and **P8** gave a response in the CV measurement. This is attributed to the greater mass fraction of glycol side chain they possess, giving them a more polar nature and allowing them to swell and uptake ions in the aqueous electrolyte better.

UV-vis absorption spectra of thin films of all polymers, spin-coated from chloroform solutions, were recorded. All polymers featured strong absorption bands in the visible region. Since performance is dictated by the nanostructure of the material, any indications of order provide insights into the structure-property relations. Noteworthy is that polymers **P1** and **P2** feature vibronic peaks around 600 nm, which suggests the presence of order in the thin film (see Figure 8b).

Grazing-incidence wide-angle X-ray scattering (GIWAXS) was performed to examine the solid-state structure of polymer films spin-coated from chloroform solutions. The polymers that provided a response in the aqueous electrolyte, **P1**, **P2**, **P3**, and **P8**, display significantly different packing behavior. The diffractograms of **P2** and **P3** feature a broad amorphous halo at q = 14.8 to 15.0 nm^{-1} (d = 0.42 to 0.43 nm). The amorphous halo has a shoulder at higher q values, which some weak π-stacking. On the other hand, **P1** and **P8** feature a clear π-stacking peak at q_{010} = 16.7 to 16.8 nm^{-1} (d_{010} = 0.36 to 0.38 nm), giving clearer evidence for ordered

domains. **P1**, **P2**, and **P8** also show lamellar stacking peaks at q_{100} of 2.87 to 3.55 nm^{-1} (d_{100} = 1.8 to 2.1 nm), confirming the presence of ordered domains. **P2** even shows a second order diffraction at q_{200} = 7.61 nm^{-1} indicating the large size of the ordered domains (see Figure 8c).

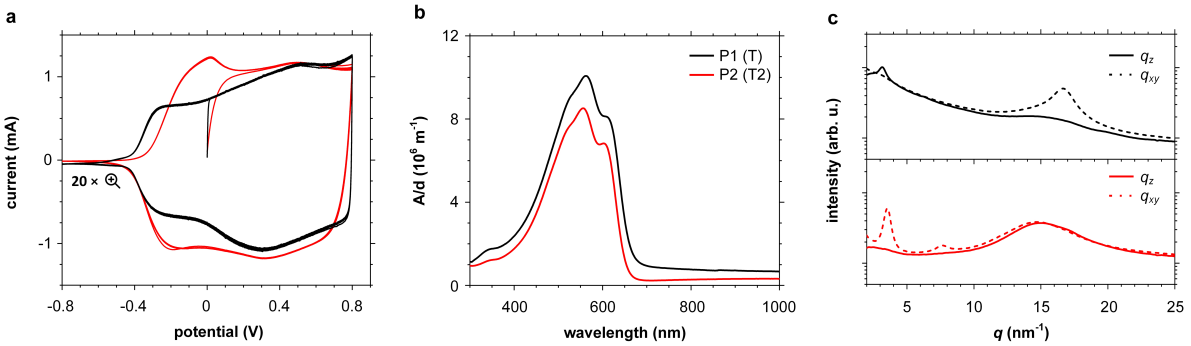

Figure 8. (a) Cyclic voltammograms measured in 0.1 M NBu_4PF_6 in acetonitrile of thin films, (b) thickness-normalized UV-vis absorption spectra (absorbance *A* divided by film thickness *d*), and (c) GIWAXS out-of-plane (q_z; solid lines) and in-plane diffractograms (q_{xy}; dashed lines) of polymers P1 (black) and P2 (red). Adapted from paper I.

4.4 Analysis of OMIEC-active materials by conventional methods

P1, **P2**, **P3**, and **P8** were tested for their output characteristics since they were the only polymers responsive in aqueous electrolyte. Owing to its low molecular weight, **P3** only showed a limited response and is not discussed further. **P1**, **P2** and **P8** showcased enhancement mode p-type operation and had negligible contact resistance between the active material and the electrodes. These materials operated in the saturation regime with a uniform source-drain current (I_{DS}) at a drain-source potential (V_{DS}) < -0.5 V, and accordingly could be studied in-depth (see Table 3 for summarized results).

By fabricating OECT devices and subsequently determining the dimension-normalized drain current I^*_{DS} and the dimension-normalized transconductance g^*_m of these devices. Then, by using Equation 4 the figure-of-merit $[\mu C^*]$ was determined:

$$\partial g_m / \partial V_{GS} = [\mu C^*] \cdot (wd/L) \quad (4)$$

where *w* and *L* are the width and length of the device channel and *d* is the active-layer thickness. For **P1** and **P2**, a $[\mu C^*]_{max}$ of 182 and 370 F cm^{-1} V^{-1} s^{-1}, respectively, was obtained whilst **P8** reached a relatively low $[\mu C^*]_{max}$ = 53 F cm^{-1} V^{-1} s^{-1}.

Volumetric capacitance C^* was determined by electrochemical impedance spectroscopy (EIS). Since the E_{ox} of **P1**, **P2**, and **P8** were comparable, the materials exhibited similar onset potentials of C^* at V_{GS} = -0.1 to 0 V. Maximum C^* of 152, 215 and 148 F cm^{-3} for **P1**, **P2** (at V_{GS} = -0.6 V) and **P8** (at V_{GS} = -0.7 V), respectively.

Mobility μ values were obtained by dividing $[\mu C^*]$ from the transfer curves by the C^* from the EIS. **P1** and **P2** feature a high μ_{max} = 1.3 and 1.8 cm^2 V^{-1} s^{-1} as opposed to **P8** which showed a significantly lower μ_{max} = 0.3 cm^2 V^{-1} s^{-1}. The higher mobility of **P1** and **P2** is attributed to the highly ordered domains as determined by the vibronic peaks in UV-vis and lamellar/π-stacking peaks in GIWAXS. The decreased mobility of **P8**, despite a similarly ordered structure in GIWAXS, is attributed to the conformational chaos and energetic mismatch within the polymer chain. Density functional theory calculations indicated that **P8** possesses much higher dihedral bond angels between the conjugated units (55°) as opposed to **P1** and **P2** (27° and 13°, respectively). Moreover, coefficients of the highest occupied molecular orbital (HOMO) of **P8** are more localized on the g$_3$TT unit. Instead, in **P1** and **P2** the HOMO is more delocalized onto the thiophene and bithiophene units.

Table 3. OECT performance. [a]Threshold voltage V_{th} obtained from OECT transfer curves. [b]Maximum value of the product of hole mobility and volumetric capacitance, $[\mu C^*]_{max}$, obtained from OECT transfer curves. [c]Maximum volumetric capacitance C^*_{max} determined through EIS. [d]Maximum hole mobility μ_{max} obtained by dividing $[\mu C^*]$ by C^*. Values in brackets denote the corresponding gate potential for each value; the mean and min-max error of the values extracted from two devices are given. Adapted from paper I.

polymer	V_{th} (V)[a]	$[\mu C^*]_{max}$ (F cm^{-1} V^{-1} s^{-1})	C^*_{max} (F cm^{-3})	μ_{max} (cm^2 V^{-1} s^{-1})
P1 (T)	−0.38 ± 0.02	168 ± 17 (−0.55 V)	>152 ± 17 (−0.6 V)	1.3 ± 0.2 (−0.5 V)
P2 (T2)	−0.35 ± 0.01	368 ± 9 (−0.55 V)	>215 ± 24 (−0.6 V)	1.8 ± 0.2 (−0.5 V)
P8 (BT)	−0.53 ± 0.01	50 ± 6 (−0.75 V)	148 ± 16 (−0.7 V)	0.3 ± 0.1 (−0.7 V)

4.5 Analysis of OMIEC-active materials by small signal analysis

By applying a small fluctuating gate electric field on the channel alongside the main voltage sweep, small differences in charge movement in the active material are created concomitantly with doping of the material. Using the real and imaginary output current values (redox and capacitive responses, respectively) plotted against the gate-source potential V_{GS}, material and device parameters could be determined from a single measurement (see Figure 9). This included: i) conductance G by using $G = I_{DS}/V_{DS}$, ii) conductivity σ by normalizing G with respect to the dimensions of the active material, iii) capacitance C (and in turn volumetric capacitance C^*) by definition of $C = dq/dV$ and capacitance depending on the imaginary part of $I_{GS} = dq/dt$, iv) transconductance g_m by definition $g_m = dI_{DS}/dV_{GS}$, v) $[\mu C^*]$ values from $g_m = [\mu C^*](wd/L)\, V_{DS}$, and vi) μ by taking into account the length of the channel L_{ch} and the transit time τ_e of charge carriers through the material at different V_{DS}. The obtained values for $[\mu C^*]$, μ and C^* are in the same range as determined with conventional techniques as per Table 3.

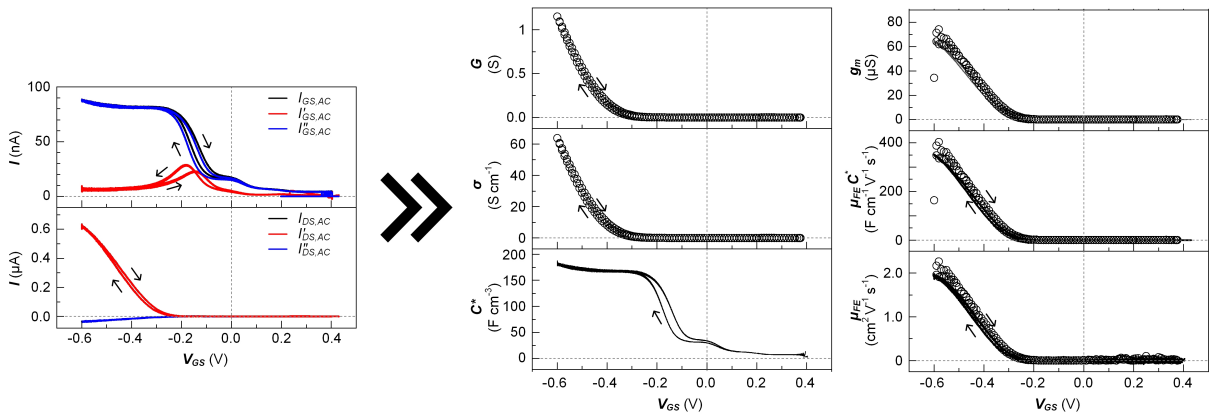

Figure 9. Small signal characterization. Left: Plots of transient gate current (upper) and drain current response (lower) as a function of the V_{GS}, obtained from the small signal characterization. The real (red) and imaginary component (blue) were extracted from the output current values (black). Right: Parameter extraction through the small signal characterization method. Traces of conductance G, conductivity σ, volumetric capacitance C^*, transconductance g_m, product of field-effect mobility and volumetric capacitance μC^*, and field-effect mobility μ_{FE} as a function of the potential of the gate electrode $V_{GS,DC}$. Adapted from paper II.

4.6 Comparison of OMIEC-active materials analysis methods

For a proper statistical analysis of the accuracy of the evaluation methods, 40 samples (prepared from the same batch of **P2**) were measured with the different methods and $[\mu C^*]$ and μ extracted. $[\mu C^*]$ for all characterization methods showed a comparable deviation of around 7.2%. However, the deviation of the mobility is significantly reduced from around 7.2% by the conventional methods to 4.1% in small signal analysis. This decrease in error was attributed to the lack of channel thickness dependence as well as the lack of propagation of errors which exists in dividing $[\mu C^*]$ by the C^* determined by EIS.

Noteworthy is the slightly lowered $[\mu C^*]$ value obtained from small signal analysis compared to the conventional methods. This is due to an underestimation of C^* – at the lower operating frequency of 10 Hz in small signal analysis, ionic motion is hampered. This is contrary to extraction of C^* by EIS, where frequency ranges from 0.1 to 10,000 Hz are used. Based on direct comparison of $[\mu C^*]$ values, the underestimation of C^* is around 10%.

Chapter 5 Conclusion and Outlook

In this thesis, novel thieno[3,2-b]thiophene-based copolymers were synthesized and tested for their performance as organic mixed ionic–electronic conductors (OMIECs) in organic electrochemical transistors (OECTs). The best material was then subjected to small signal analysis to compare this new evaluation method for OECTs.

5.1 Conclusions

By careful deliberation, the monomer 3,6-bis(triethylene glycol monomethyl ether)thieno[3,2-b]thiophene (g_3TT) was chosen as it avoided detrimental defect formation prevalent in direct arylation polymerization. Ten comonomers with differing electronic behavior (from strongly electron donating to strongly electron withdrawing) were successfully copolymerized with g_3TT. Polymers differed in their yield and molecular weight, which was attributed to steric effects within the polymer and specific side reactions of the brominated comonomers. Ultimately, the electronic character of the brominated comonomer did not influence the polymerization, showcasing the versatility of this synthetic route.

A rare feature in the polymers is observed: molecular weight can be determined by high-temperature NMR owing to the presence of end-group signals. By comparison of the g_3TT glycol chain end-groups and the g_3TT glycol chain main chain signals, molecular weight was evaluated. The values obtained by this method are in fair agreement with those obtained by size-exclusion chromatography.

A selection of the polymers obtained, namely **P1** (T), **P2** (T2), **P3** (TT), and **P8** (BT), were responsive to cyclic voltammetry in aqueous electrolyte suggesting they could be used as OMIECs in OECTs. Other polymers were not responsive since they mainly comprised aliphatic side chains and backbones (> 60% mass). Especially **P1** and **P2** were promising as OMIEC materials. Both these materials showcased high order both in UV-vis, indicated by vibronic peaks, and GIWAXS, indicated by their clear π-stacking and lamellar stacking peaks.

To evaluate the performance of the materials with other compounds in the field, as well as their associated synthetic complexity indices (SCIs), their data was plotted in an Ashby plot (see Figure 10). **P2** is one of the few compounds synthesized by DAP with a low SCI within the state-of-the-art regime, showcasing comparable figure-of-merit as Poly(3,4-ethylenedioxythiophene):poly(styrene sulfonate) (PEDOT:PSS) post-treated with sulfuric acid.

P2 was further analyzed by the novel small signal analysis, and six important parameters (conductance, conductivity, capacitance, transconductance, mobility, and transit time) simultaneously extracted with greater accuracy compared to conventional techniques.

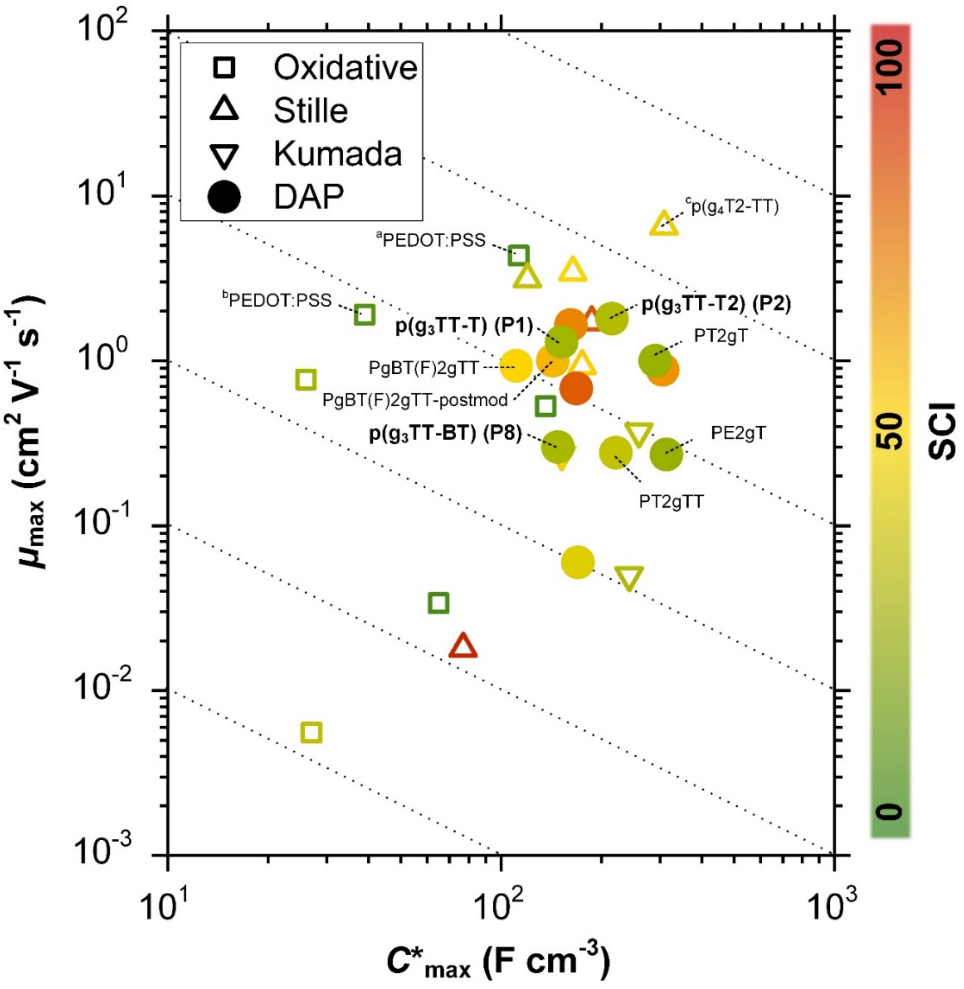

Figure 10. Ashby plot of maximum volumetric capacitance C^*_{max} and maximum charge-carrier mobility μ_{max} of previously reported p-type polymers, and selected polymers synthesized in this work (bold) by oxidative polymerization (squares), Stille coupling (upward triangles), Kumada coupling (downward triangles) or DAP (circles), with the synthetic complexity index (SCI) of each synthesis indicated by a red-green scale. [a]PEDOT:PSS post-treated with sulfuric acid, [b]PEDOT:PSS post-treated with ethylene glycol, [c]p(g4T2-TT) fractionated by size-exclusion chromatography (highest molecular weight fraction, catalyst removed). Adapted from paper I.

5.2 Outlook

Future research into this topic encompasses further improvement in the synthesis considering the synthetic complexity index. Improving the yield of each step and removal of more hazardous materials is imperative in case of further upscaling efforts. This is especially true for the polymerization step, which lags with low yields of around 30% in specific cases and uses toluene as a solvent.

The difficulty of upscaling is not exclusive to the synthesis. Large-scale production of devices also suffers from efficiency and reproducibility issues. Organic electronics benefit from improved solubility in organic solvents and accordingly upscaling effort by e.g. large-scale printing is faster than the inorganic counterparts. A selection of polymers in this work are planned to be used in inkjet printing the active material of OECTs.

ACKNOWLEDGEMENTS

I would like to express my sincerest gratitude to Prof. Christian Müller for guiding me. His advice and enthusiasm have supported me throughout the entire project. I would also like to thank Prof. Renee Kroon and Prof. Michael Sommer for their insights.

It has been a pleasure working alongside everyone on the 8th floor – from the very first moment you made me feel very welcome and I enjoy coming to work everyday thanks to you. A special thanks to Mavi, Youngseok, Mariza, and Diego (temporary 8th floor resident); the enjoyment I get from our scientific (and sometimes not so scientific) discussions is immeasurable.

A massive shout-out to Monika and Krzysztof for always lending an ear, both during and outside of worktime. I've had the best of times chatting and playing boardgames with you, and we will have many more of those opportunities in the years to come!

Daarnaast wil ik ook graag mijn familie bedanken voor alle steun die ze de laatste jaren hebben gegeven. Papa, Mama, Niels & Daniëlle, Marit & Jeffrey, en de grootouders, enorm bedankt voor alles! Ik houd zielsveel van jullie.

最後に、私のフィナンシェへ。あなたはいつまでも私の活力の源であり、私にとってのインスピレーションの源です。

BIBLIOGRAPHY

(1) *Organic Electronics Market Size And Forecast*. https://www.verifiedmarketresearch.com/product/organic-electronics-market/ (accessed 20-02-2024).
(2) Burroughes, J. H.; Bradley, D. D. C.; Brown, A. R.; Marks, R. N.; Mackay, K.; Friend, R. H.; Burns, P. L.; Holmes, A. B. Light-emitting diodes based on conjugated polymers. *Nature* **1990**, *347* (6293), 539-541. DOI: 10.1038/347539a0.
(3) Hoppe, H.; Sariciftci, N. S. Organic solar cells: An overview. *Journal of Materials Research* **2004**, *19* (7), 1924-1945. DOI: 10.1557/JMR.2004.0252.
(4) Weathers, A.; Khan, Z. U.; Brooke, R.; Evans, D.; Pettes, M. T.; Andreasen, J. W.; Crispin, X.; Shi, L. Significant Electronic Thermal Transport in the Conducting Polymer Poly(3,4-ethylenedioxythiophene). *Advanced Materials* **2015**, *27* (12), 2101-2106. DOI: 10.1002/adma.201404738.
(5) Gkoupidenis, P.; Zhang, Y.; Kleemann, H.; Ling, H.; Santoro, F.; Fabiano, S.; Salleo, A.; van de Burgt, Y. Organic mixed conductors for bioinspired electronics. *Nature Reviews Materials* **2024**, *9* (2), 134-149. DOI: 10.1038/s41578-023-00622-5.
(6) Rashid, R. B.; Ji, X.; Rivnay, J. Organic electrochemical transistors in bioelectronic circuits. *Biosensors and Bioelectronics* **2021**, *190*, 113461. DOI: 10.1016/j.bios.2021.113461.
(7) Sarkar, T.; Lieberth, K.; Pavlou, A.; Frank, T.; Mailaender, V.; McCulloch, I.; Blom, P. W. M.; Torricelli, F.; Gkoupidenis, P. An organic artificial spiking neuron for in situ neuromorphic sensing and biointerfacing. *Nature Electronics* **2022**, *5* (11), 774-783. DOI: 10.1038/s41928-022-00859-y.
(8) Giovannitti, A.; Nielsen, C. B.; Sbircea, D.-T.; Inal, S.; Donahue, M.; Niazi, M. R.; Hanifi, D. A.; Amassian, A.; Malliaras, G. G.; Rivnay, J.; et al. N-type organic electrochemical transistors with stability in water. *Nature Communications* **2016**, *7* (1), 13066. DOI: 10.1038/ncomms13066.
(9) Nielsen, C. B.; Giovannitti, A.; Sbircea, D.-T.; Bandiello, E.; Niazi, M. R.; Hanifi, D. A.; Sessolo, M.; Amassian, A.; Malliaras, G. G.; Rivnay, J.; et al. Molecular Design of Semiconducting Polymers for High-Performance Organic Electrochemical Transistors. *Journal of the American Chemical Society* **2016**, *138* (32), 10252-10259. DOI: 10.1021/jacs.6b05280.
(10) Brebels, J.; Manca, J. V.; Lutsen, L.; Vanderzande, D.; Maes, W. High dielectric constant conjugated materials for organic photovoltaics. *Journal of Materials Chemistry A* **2017**, *5* (46), 24037-24050. DOI: 10.1039/C7TA06808E.
(11) Moia, D.; Giovannitti, A.; Szumska, A. A.; Maria, I. P.; Rezasoltani, E.; Sachs, M.; Schnurr, M.; Barnes, P. R. F.; McCulloch, I.; Nelson, J. Design and evaluation of conjugated polymers with polar side chains as electrode materials for electrochemical energy storage in aqueous electrolytes. *Energy & Environmental Science* **2019**, *12* (4), 1349-1357. DOI: 10.1039/C8EE03518K.
(12) Massetti, M.; Zhang, S.; Harikesh, P. C.; Burtscher, B.; Diacci, C.; Simon, D. T.; Liu, X.; Fahlman, M.; Tu, D.; Berggren, M.; et al. Fully 3D-printed organic electrochemical transistors. *npj Flexible Electronics* **2023**, *7* (1), 11. DOI: 10.1038/s41528-023-00245-4.
(13) Sun, H.; Vagin, M.; Wang, S.; Crispin, X.; Forchheimer, R.; Berggren, M.; Fabiano, S. Complementary Logic Circuits Based on High-Performance n-Type Organic Electrochemical Transistors. *Advanced Materials* **2018**, *30* (9), 1704916. DOI: 10.1002/adma.201704916.
(14) Kukhta, N. A.; Marks, A.; Luscombe, C. K. Molecular Design Strategies toward Improvement of Charge Injection and Ionic Conduction in Organic Mixed Ionic–Electronic

Conductors for Organic Electrochemical Transistors. *Chemical Reviews* **2022**, *122* (4), 4325-4355. DOI: 10.1021/acs.chemrev.1c00266.
(15) Paulsen, B. D.; Tybrandt, K.; Stavrinidou, E.; Rivnay, J. Organic mixed ionic–electronic conductors. *Nature Materials* **2020**, *19* (1), 13-26. DOI: 10.1038/s41563-019-0435-z.
(16) Ohayon, D.; Druet, V.; Inal, S. A guide for the characterization of organic electrochemical transistors and channel materials. *Chemical Society Reviews* **2023**, *52* (3), 1001-1023, 10.1039/D2CS00920J. DOI: 10.1039/D2CS00920J.
(17) Paleti, S. H. K.; Kim, Y.; Kimpel, J.; Craighero, M.; Haraguchi, S.; Müller, C. Impact of doping on the mechanical properties of conjugated polymers. *Chemical Society Reviews* **2024**, *53* (4), 1702-1729, 10.1039/D3CS00833A. DOI: 10.1039/D3CS00833A.
(18) Inal, S.; Malliaras, G. G.; Rivnay, J. Benchmarking organic mixed conductors for transistors. *Nature Communications* **2017**, *8* (1), 1767. DOI: 10.1038/s41467-017-01812-w.
(19) Flagg, L. Q.; Bischak, C. G.; Onorato, J. W.; Rashid, R. B.; Luscombe, C. K.; Ginger, D. S. Polymer Crystallinity Controls Water Uptake in Glycol Side-Chain Polymer Organic Electrochemical Transistors. *Journal of the American Chemical Society* **2019**, *141* (10), 4345-4354. DOI: 10.1021/jacs.8b12640.
(20) Kumar Singh, V.; Mazhari, B. Measurement of threshold voltage in organic thin film transistors. *Applied Physics Letters* **2013**, *102* (25). DOI: 10.1063/1.4812191 (acccessed 2/20/2024).
(21) Hower, P. L.; Bechtel, N. G. Current saturation and small-signal characteristics of GaAs field-effect transistors. *IEEE Transactions on Electron Devices* **1973**, *20* (3), 213-220. DOI: 10.1109/T-ED.1973.17631.
(22) Hallani, R. K.; Paulsen, B. D.; Petty, A. J., II; Sheelamanthula, R.; Moser, M.; Thorley, K. J.; Sohn, W.; Rashid, R. B.; Savva, A.; Moro, S.; et al. Regiochemistry-Driven Organic Electrochemical Transistor Performance Enhancement in Ethylene Glycol-Functionalized Polythiophenes. *Journal of the American Chemical Society* **2021**, *143* (29), 11007-11018. DOI: 10.1021/jacs.1c03516.
(23) Kim, S.-M.; Kim, C.-H.; Kim, Y.; Kim, N.; Lee, W.-J.; Lee, E.-H.; Kim, D.; Park, S.; Lee, K.; Rivnay, J.; et al. Influence of PEDOT:PSS crystallinity and composition on electrochemical transistor performance and long-term stability. *Nature Communications* **2018**, *9* (1), 3858. DOI: 10.1038/s41467-018-06084-6.
(24) Rivnay, J.; Inal, S.; Salleo, A.; Owens, R. M.; Berggren, M.; Malliaras, G. G. Organic electrochemical transistors. *Nature Reviews Materials* **2018**, *3* (2), 17086. DOI: 10.1038/natrevmats.2017.86.
(25) Chujo, Y. *Conjugated Polymer Synthesis: Methods and Reactions*; John Wiley & Sons, Weinheim, 2011.
(26) He, Y.; Kukhta, N. A.; Marks, A.; Luscombe, C. K. The effect of side chain engineering on conjugated polymers in organic electrochemical transistors for bioelectronic applications. *Journal of Materials Chemistry C* **2022**, *10* (7), 2314-2332, 10.1039/D1TC05229B. DOI: 10.1039/D1TC05229B.
(27) Reynolds, J. R.; Thompson, B. C.; Skotheim, T. A. *Conjugated Polymers: Perspective, Theory, and New Materials*; CRC Press., 2019. DOI: 10.1201/b22235.
(28) Cao, Z.; Leng, M.; Cao, Y.; Gu, X.; Fang, L. How rigid are conjugated non-ladder and ladder polymers? *Journal of Polymer Science* **2022**, *60* (3), 298-310. DOI: 10.1002/pol.20210550.
(29) Cao, Z.; Li, Z.; Tolba, S. A.; Mason, G. T.; Xiong, M.; Ocheje, M. U.; Alesadi, A.; Do, C.; Hong, K.; Lei, T.; et al. Probing single-chain conformation and its impact on the optoelectronic properties of donor–accepter conjugated polymers. *Journal of Materials Chemistry A* **2023**, *11* (24), 12928-12940, 10.1039/D2TA09389H. DOI: 10.1039/D2TA09389H.

(30) Danielsen, S. P. O.; Bridges, C. R.; Segalman, R. A. Chain Stiffness of Donor–Acceptor Conjugated Polymers in Solution. *Macromolecules* **2022**, *55* (2), 437-449. DOI: 10.1021/acs.macromol.1c02229.
(31) Kroon, R.; Kiefer, D.; Stegerer, D.; Yu, L.; Sommer, M.; Müller, C. Polar Side Chains Enhance Processability, Electrical Conductivity, and Thermal Stability of a Molecularly p-Doped Polythiophene. *Advanced Materials* **2017**, *29* (24), 1700930. DOI: 10.1002/adma.201700930.
(32) Letheby, H. XXIX.—On the production of a blue substance by the electrolysis of sulphate of aniline. *Journal of the Chemical Society* **1862**, *15* (0), 161-163, 10.1039/JS8621500161. DOI: 10.1039/JS8621500161.
(33) Elschner, A.; Kirchmeyer, S.; Lovenich, W.; Merker, U.; Reuter, K. *PEDOT: Principles and Applications of an Intrinsically Conductive Polymer* CRC Press, 2010.
(34) Shi, X.; Sui, A.; Wang, Y.; Li, Y.; Geng, Y.; Wang, F. Controlled synthesis of high molecular weight poly(3-hexylthiophene)s via Kumada catalyst transfer polycondensation with Ni(IPr)(acac)2 as the catalyst. *Chemical Communications* **2015**, *51* (11), 2138-2140, 10.1039/C4CC08012B. DOI: 10.1039/C4CC08012B.
(35) Mayhugh, A. L.; Yadav, P.; Luscombe, C. K. Circular Discovery in Small Molecule and Conjugated Polymer Synthetic Methodology. *Journal of the American Chemical Society* **2022**, *144* (14), 6123-6135. DOI: 10.1021/jacs.1c12455.
(36) Rudenko, A. E.; Thompson, B. C. Optimization of direct arylation polymerization (DArP) through the identification and control of defects in polymer structure. *Journal of Polymer Science Part A: Polymer Chemistry* **2015**, *53* (2), 135-147. DOI: 10.1002/pola.27279.
(37) Elsawy, W.; Son, M.; Jang, J.; Kim, M. J.; Ji, Y.; Kim, T.-W.; Ko, H. C.; Elbarbary, A.; Ham, M.-H.; Lee, J.-S. Isoindigo-Based Donor–Acceptor Conjugated Polymers for Air-Stable Nonvolatile Memory Devices. *ACS Macro Letters* **2015**, *4* (3), 322-326. DOI: 10.1021/mz500698p.
(38) Ding, B.; Kim, G.; Kim, Y.; Eisner, F. D.; Gutiérrez-Fernández, E.; Martín, J.; Yoon, M.-H.; Heeney, M. Influence of Backbone Curvature on the Organic Electrochemical Transistor Performance of Glycolated Donor–Acceptor Conjugated Polymers. *Angewandte Chemie International Edition* **2021**, *60* (36), 19679-19684. DOI: 10.1002/anie.202106084.
(39) Halaksa, R.; Kim, J. H.; Thorley, K. J.; Gilhooly-Finn, P. A.; Ahn, H.; Savva, A.; Yoon, M.-H.; Nielsen, C. B. The Influence of Regiochemistry on the Performance of Organic Mixed Ionic and Electronic Conductors. *Angewandte Chemie International Edition* **2023**, *62* (29), e202304390. DOI: 10.1002/anie.202304390.
(40) Luo, X.; Shen, H.; Perera, K.; Tran, D. T.; Boudouris, B. W.; Mei, J. Designing Donor–Acceptor Copolymers for Stable and High-Performance Organic Electrochemical Transistors. *ACS Macro Letters* **2021**, *10* (8), 1061-1067. DOI: 10.1021/acsmacrolett.1c00328.
(41) Po, R.; Bianchi, G.; Carbonera, C.; Pellegrino, A. "All That Glisters Is Not Gold": An Analysis of the Synthetic Complexity of Efficient Polymer Donors for Polymer Solar Cells. *Macromolecules* **2015**, *48* (3), 453-461. DOI: 10.1021/ma501894w.
(42) Dolomanov, O. V.; Bourhis, L. J.; Gildea, R. J.; Howard, J. A. K.; Puschmann, H. OLEX2: a complete structure solution, refinement and analysis program. *Journal of Applied Crystallography* **2009**, *42* (2), 339-341. DOI: 10.1107/S0021889808042726.
(43) Viswamitra, M. A. Crystal Structure of Copper Ammonium Oxalate Dihydrate, Cu(NH4)2(C2O4)2·2H2O. *The Journal of Chemical Physics* **2004**, *37* (7), 1408-1414. DOI: 10.1063/1.1733297 (acccessed 1/17/2024).
(44) Yang, Q.; Zhao, Y.; Ma, D. Cu-Mediated Ullmann-Type Cross-Coupling and Industrial Applications in Route Design, Process Development, and Scale-up of Pharmaceutical and Agrochemical Processes. *Organic Process Research & Development* **2022**, *26* (6), 1690-1750. DOI: 10.1021/acs.oprd.2c00050.

(45) Cai, Q.; Zhou, W. Ullmann-Ma Reaction: Development, Scope and Applications in Organic Synthesis†. *Chinese Journal of Chemistry* **2020**, *38* (8), 879-893. DOI: 10.1002/cjoc.202000075.
(46) Barham, J. P.; Coulthard, G.; Emery, K. J.; Doni, E.; Cumine, F.; Nocera, G.; John, M. P.; Berlouis, L. E. A.; McGuire, T.; Tuttle, T.; et al. KOtBu: A Privileged Reagent for Electron Transfer Reactions? *Journal of the American Chemical Society* **2016**, *138* (23), 7402-7410. DOI: 10.1021/jacs.6b03282.
(47) Dissanayake, D. S.; Sheina, E.; Biewer, M. C.; McCullough, R. D.; Stefan, M. C. Determination of absolute molecular weight of regioregular poly(3-hexylthiophene) by 1H-NMR analysis. *Journal of Polymer Science Part A: Polymer Chemistry* **2017**, *55* (1), 79-82. DOI: 10.1002/pola.28354.
(48) Wackerly, J. W.; Dunne, J. F. Synthesis of Polystyrene and Molecular Weight Determination by 1H NMR End-Group Analysis. *Journal of Chemical Education* **2017**, *94* (11), 1790-1793. DOI: 10.1021/acs.jchemed.6b00814.
(49) Giovannitti, A.; Nielsen, C. B.; Rivnay, J.; Kirkus, M.; Harkin, D. J.; White, A. J. P.; Sirringhaus, H.; Malliaras, G. G.; McCulloch, I. Sodium and Potassium Ion Selective Conjugated Polymers for Optical Ion Detection in Solution and Solid State. *Advanced Functional Materials* **2016**, *26* (4), 514-523. DOI: 10.1002/adfm.201503791.
(50) Moser, M.; Savagian, L. R.; Savva, A.; Matta, M.; Ponder, J. F., Jr.; Hidalgo, T. C.; Ohayon, D.; Hallani, R.; Reisjalali, M.; Troisi, A.; et al. Ethylene Glycol-Based Side Chain Length Engineering in Polythiophenes and its Impact on Organic Electrochemical Transistor Performance. *Chemistry of Materials* **2020**, *32* (15), 6618-6628. DOI: 10.1021/acs.chemmater.0c02041.
(51) Ding, B.; Jo, I.-Y.; Yu, H.; Kim, J. H.; Marsh, A. V.; Gutiérrez-Fernández, E.; Ramos, N.; Rapley, C. L.; Rimmele, M.; He, Q.; et al. Enhanced Organic Electrochemical Transistor Performance of Donor–Acceptor Conjugated Polymers Modified with Hybrid Glycol/Ionic Side Chains by Postpolymerization Modification. *Chemistry of Materials* **2023**, *35* (8), 3290-3299. DOI: 10.1021/acs.chemmater.3c00327.
(52) Ding, B.; Le, V.; Yu, H.; Wu, G.; Marsh, A. V.; Gutiérrez-Fernández, E.; Ramos, N.; Rimmele, M.; Martín, J.; Nelson, J.; et al. Development of Synthetically Accessible Glycolated Polythiophenes for High-Performance Organic Electrochemical Transistors. *Advanced Electronic Materials n/a* (n/a), 2300580. DOI: 10.1002/aelm.202300580.
(53) McCulloch, I.; Heeney, M.; Bailey, C.; Genevicius, K.; MacDonald, I.; Shkunov, M.; Sparrowe, D.; Tierney, S.; Wagner, R.; Zhang, W.; et al. Liquid-crystalline semiconducting polymers with high charge-carrier mobility. *Nature Materials* **2006**, *5* (4), 328-333. DOI: 10.1038/nmat1612.